Letter Vol. 4, No. 12 / December 2017 / Optica 1488

Visual acuity in two-photon infrared vision

Pablo Artal,[1,*] Silvestre Manzanera,[1] Katarzyna Komar,[2,3] Adrián Gambín-Regadera,[1] and Maciej Wojtkowski[3,4]

[1]Laboratorio de Óptica, Universidad de Murcia, Campus de Espinardo (Edificio 34), Murcia 30100, Spain
[2]Institute of Physics, Faculty of Physics, Astronomy and Informatics, Nicolaus Copernicus University, Grudziadzka 5, 87-100 Torun, Poland
[3]Baltic Institute of Technology, Zwyciestwa 96/98, 81-451 Gdynia, Poland
[4]Institute of Physical Chemistry, Polish Academy of Sciences, Warsaw, Poland
*Corresponding author: pablo@um.es

Received 18 July 2017; revised 3 November 2017; accepted 4 November 2017 (Doc. ID 302795); published 30 November 2017

Humans can detect infrared light at wavelengths over 1000 nm, perceived as visible light of the corresponding half wavelength. This is due to a two-photon (2P) absorption process, which requires sufficiently large amounts of luminous energy. For safety reasons, this energy must be delivered by pulsed light sources well focused in the retina. Although this effect has been known for several decades, the spatial properties of 2P vision in comparison to normal vision have not yet elucidated. We have developed a new experimental system to measure, for the first time, to the best of our knowledge, visual acuity mediated by 2P absorption and compare it against that with visible light. The spatial resolution of 2P infrared vision is the same as in normal visible light. However, the use of 2P infrared vision may have some future potential applications, for example, in permitting vision in those cases with opaque optical media to visible wavelengths while keeping some transparency in the infrared.

OCIS codes: (330.1070) Vision - acuity; (190.7110) Ultrafast nonlinear optics; (190.1900) Diagnostic applications of nonlinear optics; (330.5370) Physiological optics; (330.6130) Spatial resolution.

https://doi.org/10.1364/OPTICA.4.001488

Commonly, human visual perception of electromagnetic radiation is considered restricted to its so-called visible region: 400–700 nm. This is not the whole truth since the sensitivity of the human retina goes farther in the infrared, although it is largely attenuated. The central fovea decreases from a maximum sensitivity at 550 nm toward longer wavelengths—the sensitivity relative to the maximum is reduced by a factor $\times 10^{-2.6}$ and $\times 10^{-9.5}$ at 700 nm and 1000 nm, respectively [1]. This is the reason why beams originating from light sources with wavelengths above 700 nm can be perceived by observers, particularly when they are intentionally introduced into an eye as in scanning laser ophthalmoscopes or other ophthalmic devices. In addition, during the last decades of use of pulsed infrared laser beams (ranging from 800 to 1300 nm), numerous observers perceived visible light when exposed to those beams (generating a color perception like light of half the used wavelength) [2–12]. Since the pulse shortening increased the perceived intensities of such beams, the nonlinear optical phenomena have been proposed as its explanation: second-harmonic generation either in anterior [10,13,14] or posterior [4,11] eye segments or two-photon (2P) absorption in cone's and rod's photopigments [3,5–9,12].

A recent study [12] of pulsed infrared laser beam perception provided evidence that 2P absorption in visual pigments is the most probable cause for this visual effect. Short-pulsed infrared beams activated mouse photoreceptors by nonlinear optical processes and caused photoisomerization of purified pigments and a model chromophore compound; the experimental observations from human and mice were consistent with a quantum mechanical model for 2P activation of rhodopsin. Since, by means of this 2P absorption, the IR radiation can be perceived, the capability of infrared light to penetrate deeper into the scattering media might be used, for instance, to test retinal responses in eyes suffering from severe cataracts. In this case, this could be combined with retinal imaging through ophthalmoscopes able to penetrate the lens opacifications, as that using the single-pixel approach [15], to provide a better evaluation not only of the retina but of the neural pathways.

On the other hand, multiphoton imaging has proved to be advantageous over traditional one-photon imaging techniques [16–18]. One of the reasons is that the collected signal arises only from the small volume within the center of the focal spot where the nonlinear effects take place. Such spatial confinement leading to better image quality is one of the reasons for the contemporary attractiveness of nonlinear optical processes in microscopy. The first impression of the authors of this Letter, after seeing this visual phenomenon, was like this feature of multiphoton imaging. The clarity and sharpness of the infrared-induced stimulus seems to appear higher than the visible one. The only source of perception is the focal spot for which the photon flux is sufficiently high to produce a 2P absorption process. Such a reduction in the focal spot was expected to induce an improvement in visual acuity. However, in the range of visible wavelengths, visual acuity is not only affected by optical conditions (pupil diameter, aberrations) but also retinal (sampling of the photoreceptor mosaic, retinal circuitry) and neural factors [19]. Then, whether this 2P

vision might lead to a better visual acuity in comparison with ordinary vision was subject to debate and required a dedicated new experiment.

Although there is a range of what is considered normal, most subjects achieve a letter resolution better than 1 min of arc (equivalent to 20/20). We set an experiment where visible and infrared letters were projected (point scanning) in an indistinguishable fashion to the subjects. The optical effects were minimized and equalized by using a small aperture, reducing the effect of aberrations in the retinal image [20,21]. To the best of our knowledge, the experiment reported here is the first to measure the visual resolution in 2P infrared vision to be compared with that under normal visible conditions.

A schematic diagram of the optical setup is shown in Fig. 1. The IR source was a femtosecond laser (HighQ-2, Spectra-Physics, Santa Clara, CA, USA), which delivers light pulses at the central wavelength of 1043 nm with a FWHM of 6 nm and a repetition rate of 63 MHz. The pulse temporal width at the eye's pupil plane was 435 fs after passing a 5 m fiber patch cable (P3-980A-FC-5 Thorlabs, Newton, NJ, USA) as measured with an autocorrelator. This contributed to reduce the peak power in the retina. The visible light was provided by a He–Ne continuous laser emitting at 543 nm, which is close to half the wavelength of the IR source. The color perception elicited by both the normal vision in visible and the 2P vision in IR was almost indistinguishable. To control the power delivered, different intensity attenuators are placed after the exit aperture of each of the light sources, consisting in a combination of neutral density filters (NDFs) and crossed linear polarizers (C-Pol). Output power from each source is then coupled into single-mode optical fibers (P1-460B-FC-1 Thorlabs, in the case of visible light). The use of fiber patch cables for both visible and IR allows us to filter the beams and produce high-quality point-like sources. In the case of IR, the purpose was also to avoid too short pulses and, in consequence, too high energy peaks that may be hazardous. Next, the collimated fibers' output collinearly enters the optical setup through a short-pass dichroic mirror (DM) with a cutoff wavelength at 805 nm. A variable aperture (A1) is used to limit the beam diameter entering the eye and is optically conjugated with the 2D scanning galvo mirror system (xyG) (Thorlabs) through the 1:1 optical relay composed of lenses L1 and L2. Lenses L3 and L4 form a second 1:1 optical relay, conjugating the scanning mirrors with the eye's pupil plane. All lenses are achromatic doublets. Adequate control over the galvo mirrors allows us to produce a scanning beam onto the retina to provide visual stimuli to the subject. Retinal stimulation can be halted by an additional aperture (A2), which blocks the beam after proper deflection by the galvo mirrors. We also determine the optical retinal image quality at both wavelengths by using an additional optical path to record double-pass (DP) images [22]. It consists of a beam splitter (BS), an imaging lens (L5), and an EM-CCD camera (Ixon Ultra 888-U3-CSO. Andor Technology, Belfast, UK) (CAM1). DP images were recorded through an artificial pupil of 2 mm, limited by aperture A3.

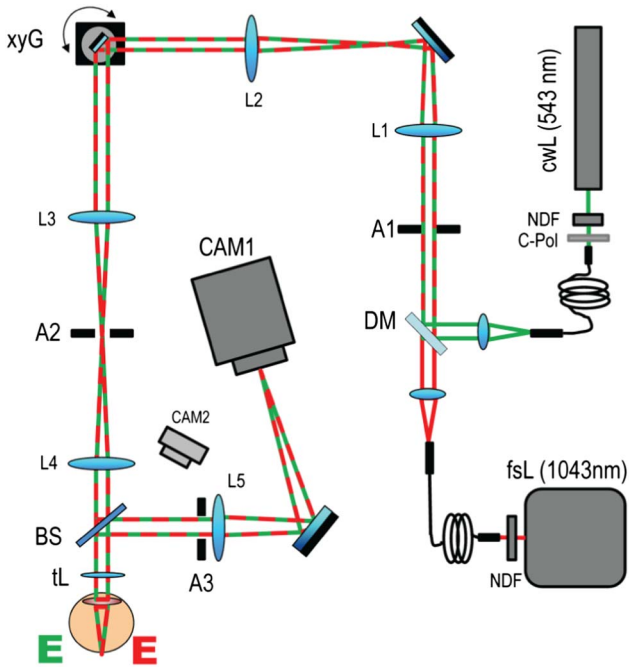

Fig. 1. Schematic diagram of the apparatus. Either a visible CW (cwL) or an IR pulsed (fsL) laser is used to deliver visual stimuli to the subject's eye by means of a galvo mirror system (xyG). Double-pass images are acquired using high-sensitivity (CAM1). Additional elements are: DM, dichroic mirror; A1–A3, apertures; L1–L5, achromatic doubles; BS, beam splitter; tL, trial lenses; NDF, neutral density filter; C-Pol, crossed linear polarizers; CAM2, alignment camera.

Proper positioning of the subject's eye relative to the instrument is achieved by means of an auxiliary camera (CAM2), and defocus and astigmatism were corrected using appropriate trial lenses (tL) placed in front of the eye. A single computer controls all the components in the setup, including the pulsed laser, the cameras, and the scanning system. Custom software was developed to implement the visual acuity (VA) test.

VA was measured for each wavelength for a range of defocus values (>3 D) induced by placing trial lenses in front of the eye in steps of 0.5 D. Natural accommodation was paralyzed in the subjects by instilling a 1% tropicamide solution. VA was measured using a tumbling E letter following a subjective adjustment procedure. In this type of procedure, subjects can freely change, by means of a keypad, the size of the letter and finally select the size corresponding to his/her discrimination threshold. Each time the subject changed the letter size, a new letter was presented for 300 ms with a random orientation. At each focus position, VA was measured three times. For visible and IR light, VA was estimated using 1.0 mm and 2.0 mm aperture diameters, respectively. This assured that the size of the scanning spot on the retina, which was basically diffraction limited, was the same for both visible and IR light.

The brightness of the stimulus generated in visible light was subjectively optimized to have the best resolution. It was performed by producing an E letter and modifying the laser power until the image was perceived as the sharpest.

The laser power measured at the pupil plane was 0.8 pW. The maximum permissible power entering the eye for this beam, calculated based on the ANSI Z136.1-2014, was 480 nW for 1890 s exposure ($t = 90$ s/meas. × 3 meas./focus × 7 focus = 1890 s). To match the perceived luminance of the letter in visible light, the power of the IR source was subjectively adjusted as well. To this end, both letters were presented simultaneously shifted one relative to the other. Following this procedure, the delivered power at the eye's pupil plane in IR was set at 79 μW. This was always well below the ocular safety limits imposed by the ANSI Z136.1-2014. As a reference, for a stationary spot with

exposure duration in the range of 10–30,000 s, the maximum permissible power entering the eye is limited to 1.89 mW for that wavelength, treating experimental conditions as purposeful starting conditions (paragraph 8.2.2 ANSI) and calculating maximum permissible exposure (MPE) for the time of 10 s. A more restrictive approach is treating our experiment as unusual viewing conditions with, to a certain degree, a constrained eye by using tropicamide drops. Then, MPE calculated for 1890 s for the 1043 nm beam is equal to 510 μW. Notice that the VA measurements were performed using a flying spot, which always increases the MPE values.

The Supplement 1 presents detailed information on how the calculations were performed to establish the exposure safety limits accordingly to the ANSI safety rules for all the light sources used and all the experimental conditions.

Since there is a significant difference in wavelength (500 nm) between the visible and the IR radiations employed, the magnitude of the potential longitudinal chromatic aberration (LCA) of the optical setup was carefully evaluated. Two are the main sources of LCA: the achromatic doublets (L1–L5) and the trial lenses. We estimated that the combination of the four achromatic doublets (L1–L4) induces a LCA of 0.14 D and L5 0.02 D. The trial lenses show a linear relationship between the induced LCA and the optical power of the lens (slope of −0.07). This relationship was obtained using the values of the refractive index of the lenses' material for visible and IR and the measurements of the radius of curvature of the lenses. These values of LCA were later applied to assess the actual defocus induced using IR radiation.

Six healthy volunteers with ages ranging from 26 to 55 years and with no record of previous ocular diseases participated in the experiment. Except for two mildly myopic subjects, the remaining subjects were emmetropic. Only one of the participants showed astigmatism above 0.25 D and was corrected. The characteristics and potential risks of the experiment were explained, and the participants signed informed consent forms. The study followed the tenets of the Declaration of Helsinki and was approved by the University of Murcia ethics committee.

Through-focus VA was measured in both visible and 2P-IR. For each subject, defocus was expressed relative to the focus position where the best VA in visible was obtained and using this reference the through-focus VA was averaged across subjects. Figure 2 shows the VA results.

The average best VA was not substantially different when measured either in visible or in 2P-IR light. The best VA for visible is 1.03 ± 0.21 and for IR is 1.02 ± 0.14 min of arc. We found a focus shift in the location of the best VA between visible and IR of 1.5 D. The estimate of the chromatic difference in focus between 543 nm and 1043 nm from previous studies' data [23,24] was 1.4 D. Considering the sampling in defocus used in our study, this value is in good agreement with the focus shift we found and may be fully considered a consequence of the eye's chromatic aberration.

Through-focus DP images were recorded within a 3 D defocus range centered on the focus position achieving the best VA, aiming at locating the best focused image. To acquire these images, the scanning was halted and photons reflected from the subject's retina accumulated for 4.2 s in the case of visible light and 2.1 s in the case of IR. The exposure duration for the visible light was longer due to the lower reflectivity of the retina and to the lower incident power used (1.2 μW versus 70 μW for the IR). In both cases, this was below the ANSI limits (VIS: 10.3 μW for a total exposure duration of 21 s; IR: 1.3 mW for 42 s). Figure 3 shows an example of the best focused images acquired for both the visible and the IR from one of the subjects. Figure 2 (open symbols) shows the averaged across subjects through-focus maximum intensity in the image. This intensity is provided by the camera in the form of the number of photon counts at each pixel. Among the through-focus sequence of images, the best focused image is selected as the one showing the greatest maximum intensity. The best focused images were found to be located at 0 and 1.5 D for visible and IR light, respectively. The comparison between the through-focus VA and the maximum intensity reveals that the best VA and the best focused image are obtained at the same focus position. This implies that the retinal layer sensitive to light (plane of vision) and the one reflecting most of the optical radiation employed to acquire the DP images (plane of reflection) are coincident within a certain uncertainty interval. Considering that defocus was sampled in steps of 0.5 D, this uncertainty interval can be estimated (using the Emsley's reduced eye model [25]), as approximately 138 μm. This coincidence of the planes of vision and reflection in visible light was previously reported [26].

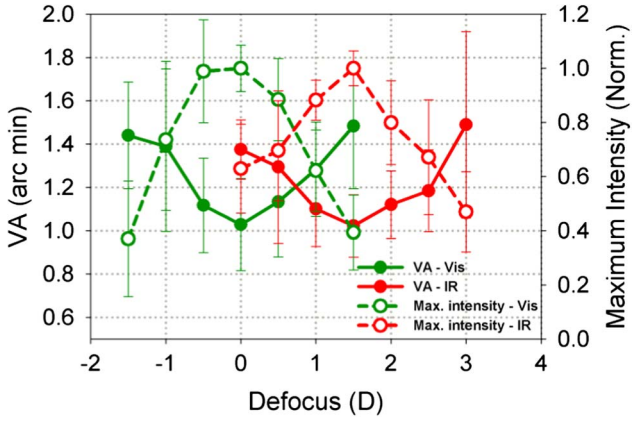

Fig. 2. On the left, the Y axis (solid lines) is represented by the averaged visual acuity across subjects measured in visible and IR light as a function of defocus. Values are shown normalized to the maximum. All defocus values are relative to the focus position where the best VA is achieved in visible light. Error bars stand for intersubject variability. See Data File 1 for underlying values. On the right Y axis (dashed lines and open symbols), the averaged-across-subjects through-focus maximum intensity in the recorded double-pass images.

In conclusion, we measured, for the first time, to the best of our knowledge, the visual acuity of infrared 2P vision. It was found to be the same as for visible light at best focus (shifted accordingly for chromatic aberration). Double-pass retinal images were more extended in IR due to a deeper penetration within the retina (see Fig. 3), although this diffuse IR light did not affect visual resolution. Further, the minimum in the VA curves coincides with the maximum of intensity for the through-focus DP images. These results support a retinal origin of 2P vision phenomenon.

This capability of producing visual perception using IR light could be exploited in some applications. 2P-IR vision would require scanning the short-pulsed laser spot over the retina. This could be incorporated in an ophthalmic instrument to evaluate the condition of the visual system in nearly opaque eyes.

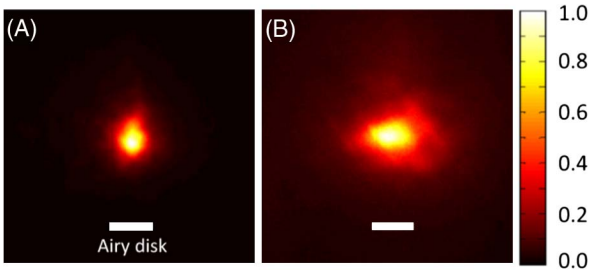

Fig. 3. Example of the recorded double-pass images. They correspond to the best focused images recorded from subject #4 in (A) visible and (B) IR. They are normalized to the maximum. The width of each scale bar represents the corresponding Airy disk diameter for the wavelength and pupil size used (4.6 and 4.4 min of arc for visible and IR, respectively).

Other possible uses that require further investigations may include early detection of retinal diseases by testing thresholds of visible perception for pulsed IR beams.

Funding. FP7 Ideas: European Research Council (IDEAS-ERC) (ERC-2013-AdG-339228); Secretaría de Estado de Investigación, Desarrollo e Innovación (SEIDI) (FIS2016-76163-R); Fundación Séneca (f SéNeCa) (19897/GERM/15); European Regional Development Fund (ERDF); Narodowe Centrum Nauki (NCN) (2016/23/B/ST2/00752); City of Gdynia (3/DOT/216); Horizon 2020 Framework Programme (H2020) (666295).

See Supplement 1 for supporting content.

REFERENCES

1. D. R. Griffin, R. Hubbard, and G. Wald, J. Opt. Soc. Am. **37**, 546 (1947).
2. L. S. Vasilenko, V. P. Chebotaev, and Y. Troitskii, Sov. Phys. JEPT **21**, 513 (1965).
3. B. M. Savin, R. I. Kovach, and E. E. Kolchin, Dokl. Akad. Nauk SSSR **221**, 225 (1975).
4. D. H. Sliney, R. T. Wangemann, J. K. Franks, and M. L. Wolbarsht, J. Opt. Soc. Am. **66**, 339 (1976).
5. B. M. Savin and E. E. Kolchin, Dokl. Akad. Nauk SSSR **1**, 235 (1977).
6. V. G. Dmitriev, V. N. Emel'yanov, M. A. Kashintsev, V. V. Kulikov, A. A. Solov'ev, M. F. Stel'makh, and O. B. Cherednichenko, Sov. J. Quantum Electron. **9**, 5 (1979).
7. V. Y. Prokopyev, Biofizika **25**, 305 (1980).
8. V. Y. Prokopyev, Biofizika **25**, 2 (1980).
9. V. Y. Prokopyev, Biofizika **30**, 4 (1985).
10. T. Theodossiou, E. Georgiou, V. Hovhannisyan, and D. Yova, Lasers Med. Sci. **16**, 34 (2001).
11. P. V. Kazakevich, A. V. Simakin, and G. A. Shafeev, Laser Phys. **16**, 1078 (2006).
12. G. Palczewska, F. Vinberg, P. Stremplewski, M. P. Bircher, D. Salom, K. Komar, J. Zhang, M. Cascella, M. Wojtkowski, V. J. Kefalov, and K. Palczewski, Proc. Natl. Acad. Sci. USA **111**, E5445 (2014).
13. S. Fine and W. P. Hansen, Appl. Opt. **10**, 2350 (1971).
14. Q. Zaidi and J. Pokorny, Appl. Opt. **27**, 1064 (1988).
15. B. Lochocki, A. Gambín, S. Manzanera, E. Irles, E. Tajahuerce, J. Lancis, and P. Artal, Optica **3**, 1056 (2016).
16. W. R. Zipfel, R. M. Williams, R. Christie, A. Y. Nikitin, B. T. Hyman, and W. W. Webb, Proc. Natl. Acad. Sci. USA **100**, 7075 (2003).
17. Y. Imanishi, M. L. Batten, D. W. Piston, W. Baehr, and K. Palczewski, J. Cell Biol. **164**, 373 (2004).
18. J. M. Bueno, E. J. Gualda, and P. Artal, J. Biomed. Opt. **15**, 066004 (2010).
19. P. Artal, Adv. Opt. Photon. **6**, 340 (2014).
20. P. Artal, E. Berrio, A. Guirao, and P. Piers, J. Opt. Soc. Am. A **19**, 137 (2002).
21. P. Artal and J. Tabernero, Nat. Photonics **2**, 586 (2008).
22. J. Santamaría, P. Artal, and J. Bescós, J. Opt. Soc. Am. A **4**, 1109 (1987).
23. L. N. Thibos, M. Ye, X. Zhang, and A. Bradley, Appl. Opt. **31**, 3594 (1992).
24. E. J. Fernández, A. Unterhuber, P. M. Prieto, B. Hermann, W. Drexler, and P. Artal, Opt. Express **13**, 400 (2005).
25. H. H. Emsley, *Visual Optics* (Butterworths, 1952).
26. E. A. Villegas, C. González, B. Bourdoncle, T. Bonnin, and P. Artal, Opt. Vis. Sci. **79**, 60 (2002).